FGF5 is a crucial regulator of hair length in humans

Claire A. Higgins[a,1,2], Lynn Petukhova[a,b,1], Sivan Harel[a], Yuan Y. Ho[a], Esther Drill[a], Lawrence Shapiro[c], Muhammad Wajid[a,d], and Angela M. Christiano[a,e,3]

Departments of [a]Dermatology, [b]Epidemiology, [c]Biochemistry and Molecular Biophysics, and [e]Genetics and Development, Columbia University, New York, NY 10032; and [d]University of Education, Okara Campus, Lahore, Pakistan

Edited by Stephen T. Warren, Emory University School of Medicine, Atlanta, GA, and approved April 22, 2014 (received for review February 14, 2014)

Mechanisms that regulate the growth of eyelashes have remained obscure. We ascertained two families from Pakistan who presented with familial trichomegaly, or extreme eyelash growth. Using a combination of whole exome sequencing and homozygosity mapping, we identified distinct pathogenic mutations within fibroblast growth factor 5 (*FGF5*) that underlie the disorder. Subsequent sequencing of this gene in several additional trichomegaly families identified an additional mutation in *FGF5*. We further demonstrated that hair fibers from forearms of these patients were significantly longer than hairs from control individuals, with an increased proportion in the growth phase, anagen. Using hair follicle organ cultures, we show that FGF5 induces regression of the human hair follicle. We have identified FGF5 as a crucial regulator of hair growth in humans for the first time, to our knowledge, and uncovered a therapeutic target to selectively regulate eyelash growth.

hair cycling | catagen | next-generation sequencing | consanguineous families

Hair follicles are a unique mammalian organ because they go through continuous cycles of growth (anagen), regression (catagen), and rest (telogen) throughout their lifetime (1). In humans, different body sites such as the eyelashes, torso, or scalp grow hair fibers to a variety of lengths and contain follicles with varying anagen:telogen ratios. For example, on the scalp, there is a high anagen:telogen ratio with follicles residing in anagen for several years, but remaining in telogen for just 3 mo, resulting in growth of long hair. In contrast, hairs on other body sites, such as the arms, thighs, or eyelashes, have a short anagen duration (weeks), followed by a comparatively long telogen (months), resulting in the growth of shorter hairs on these sites (2, 3). Little is known about the molecular regulators that determine short versus long hair in humans, and yet this is clearly a quantitative trait that varies between individuals and sometimes within families, suggesting inherited differences.

To gain insight into the genetic regulators of hair fiber length, we performed homozygosity mapping combined with whole exome sequencing in two consanguineous families from Pakistan who presented with familial trichomegaly (FT) (or excessively long eyelashes) (Online Mendelian Inheritance in Man database, OMIM 190330). The term "trichomegaly" was first coined by Gray in 1944, to describe the growth of very long eyelashes, also termed "movie lashes," because these were particularly desirable by women in Hollywood (4). Whereas several cases of trichomegaly have been reported as acquired, or as an off-target drug effect (5), familial trichomegaly is rare, with only a couple of described cases (6). We ascertained 21 members of family 1 (FT1), and 9 members of family 2 (FT2), who presented with familial trichomegaly consistent with an autosomal recessive trait (Fig. 1 *A* and *B*). In members of both FT1 and FT2, the extreme eyelash growth observed is striking (Fig. 1 *C* and *D*, and Fig. S1); however, other ectodermal appendages including nails and teeth had no obvious abnormalities.

Results

Identification of Causative Mutations in Fibroblast Growth Factor 5. We performed genome-wide SNP genotyping on 14 members of FT1 to identify evidence for regions with linkage and homozygosity. Whereas SNP data for FT1 was uninformative for linkage, a maximum homozygosity score of 84 was obtained for a single region on chromosome 4q21.21 (Fig. 2 *A* and *B*), indicating a large continuous region of homozygous genotypes shared among affected individuals and not present in unaffected ones (7). Because exome sequencing has rapidly emerged as a powerful means to identify genes that cause rare Mendelian phenotypes, we simultaneously performed whole exome sequencing on two members of FT1, three members of FT2, and five unaffected ethnically matched controls. To identify variants that were consistent with our disease model, we used a filtering strategy in which we excluded (*i*) any variants heterozygous in one or more affected individuals; (*ii*) variants not present in all affected family members; (*iii*) variants present in unaffected ethnically matched controls; or (*iv*) variants annotated in public databases, including 1000 Genomes Project and the National Heart Lung and Blood Exome Variant Server containing exome data from 6,500 individuals. Using this filtering strategy, we identified a single gene, fibroblast growth factor 5 (*FGF5*), which resides on chromosome 4q21.21, directly within the region of homozygosity, and which harbored previously unidentified homozygous mutations in both our families (Fig. 2*C*).

In FT1, we identified a 1-base pair (bp) deletion at the donor splice site of intron 2 (c.459+1delG), whereas in FT2 we identified a 2-bp deletion within exon 1 (c.159_160delTA). Sanger sequencing was used to validate these mutations (Fig. S2), which demonstrated significant evidence for cosegregation in both families with a logarithm of odds (LOD) score of 5.73. We next

Significance

Hair length varies dramatically on different body sites and also varies between individuals. Thus, hair length is a quantitative trait, suggesting inherited differences. In this study, we obtained DNA from families segregating excessively long eyelashes consistent with an autosomal recessive trait. We identified mutations in a single gene, fibroblast growth factor 5 (*FGF5*), which was homozygous in affected family members only. FGF5 has previously been implicated as a regulator of hair lengths in mammals, with mutations resulting in the well-described *angora* phenotype. However, until now a human counterpart to this phenotype remained elusive. Here, we present, to our knowledge, the first human counterpart of the *angora* phenotype, showing that FGF5 underlies trichomegaly and is a crucial regulator of hair growth in humans.

Author contributions: C.A.H., L.P., and A.M.C. designed research; C.A.H., L.P., S.H., Y.Y.H., E.D., and L.S. performed research; L.S. and M.W. contributed new reagents/analytic tools; C.A.H., L.P., S.H., Y.Y.H., E.D., L.S., and A.M.C. analyzed data; and C.A.H., L.P., S.H., and A.M.C. wrote the paper.

The authors declare no conflict of interest.

This article is a PNAS Direct Submission.

[1]C.A.H. and L.P. contributed equally to this work.

[2]Present address: Department of Bioengineering, Imperial College London, London SW7 2AZ, United Kingdom.

[3]To whom correspondence should be addressed. E-mail: amc65@columbia.edu.

This article contains supporting information online at www.pnas.org/lookup/suppl/doi:10.1073/pnas.1402862111/-/DCSupplemental.

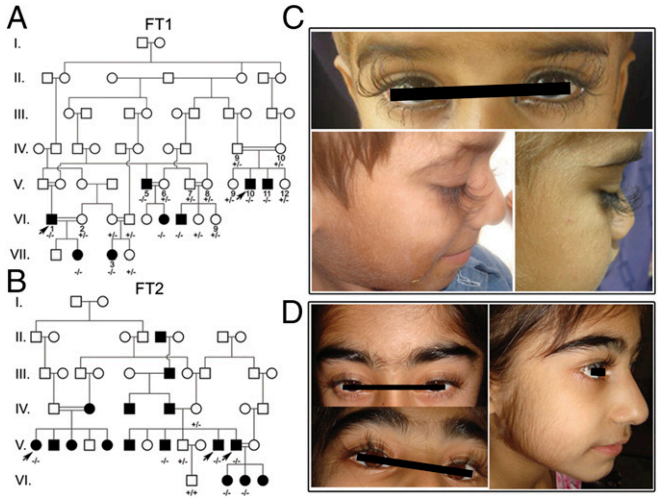

Fig. 1. Pedigrees and clinical presentation of trichomegaly. Pedigree for FT1 (*A*) and FT2 (*B*). Filled symbols represent affected individuals, whereas unfilled represent unaffected. DNA samples available at the start of our study, and used for homozygosity mapping in FT1, are numbered on the pedigree. Arrows indicate samples used for whole exome sequencing, while samples used for Sanger sequencing analysis, and LOD score calculation have genotypes indicated below (+, reference sequence, –, mutation). (*C*) Clinical presentation of FT1 family members. Trichomegaly is visually striking, with family members exhibiting extremely long eyelashes. All family members in these photographs are prepubescent; however, individuals remain affected throughout their lifetime. (*D*) Clinical presentation of FT2 family members indicates trichomegaly with mild hypertrichosis on the cheeks, forehead. and eyebrows. Hypertrichosis on the face is due to an increased length of vellus hair follicles rather than a vellus to terminal switch, indicating a prolonged duration of anagen within these follicles. In nails and other ectodermal appendages, no obvious abnormalities were identified.

sequenced *FGF5* in unrelated probands from five additional FT families and identified an additional homozygous missense mutation in exon 3 (c.520T > C), in a single proband (FT3) from Pakistan (Fig. 2*D*). Using the rare variant burden test (8), we calculated that the number of rare damaging mutations in *FGF5* identified in our cohort is greater than expected by chance ($P = 4.5 \times 10^{-10}$). None of the identified mutations were present in 50 ethnically matched controls, nor have they been reported in any public database. The fraction of familial trichomegaly cases caused by mutations in *FGF5* is 42.5% (3/7) in this study.

Protein Consequences of FGF5 Mutations. *FGF5* is subject to alternative splicing, which generates two *FGF5* transcripts, one producing a 268-amino-acid protein (FGF5), and a second, shorter 123-amino-acid protein, FGF5-short form (FGF5S). In *FGF5S*, exon 2 is skipped, and a frameshift due to the out-of-frame splicing of exon 1 to exon 3 results in translation of only 14 base pairs of exon 3 before a termination codon (Fig. S3). FGF5 contains a conserved receptor binding domain whose coding sequence spans all three exons, and interacts with its receptor, FGFR1 (9, 10). Moreover, FGF5S has been shown to act in an antagonistic manner by competitively binding FGFR1, preventing activation of FGFR1 by FGF5 (11). The mutation in FT2 is located within exon 2 and causes a frameshift affecting both FGF5 and FGF5S, whereas the mutations observed in FT1, and FT3 reside in exons 2 and 3, respectively, and therefore only affect full-length FGF5. In FT3 (Fig. 3*A*), the missense mutation (c.520T > C) converts a conserved tyrosine residue to histidine (p.Y174H). Examination of FGF-FGFR cocrystal structures (12, 13) shows that Y174 is positioned within a hydrophobic core and resides adjacent to several receptor-interaction surfaces where it likely stabilizes them in their native conformation (Fig. 3 *B* and *C*). We used the functional prediction programs Polyphen-2, SIFT, and Mutation Assessor (14–16) to determine the effect of the missense mutation in FT3. Polyphen-2 (14) predicted the change would be "probably damaging" with a score of "1"; SIFT (16) predicted the mutation would be "deleterious" with a score of "0"; whereas Mutation Assessor (15) indicated the functional impact of the mutation was "high," within a disease-causing range, with an impact score of 3.535. Taken together, these predictions suggest that p.Y174H is likely to have a negative impact on the function of FGF5. We predict that substitution of the hydrophobic side chain of tyrosine with a hydrophilic histidine is likely to impact the function of FGF5 such that it would

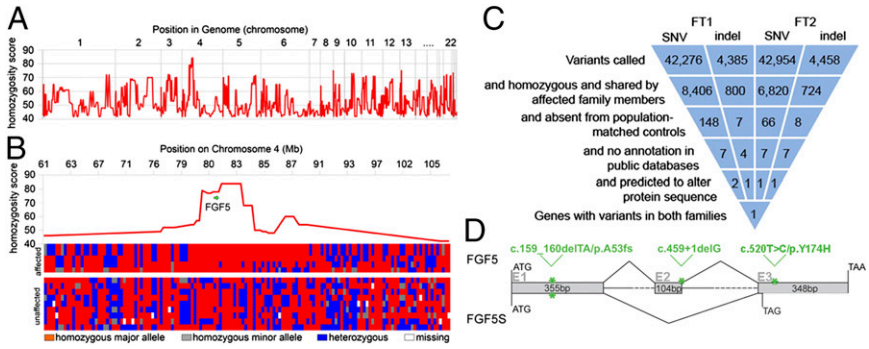

Fig. 2. Combined homozygosity mapping and whole exome sequencing strategy for identification of *FGF5*. (*A*) Genome-wide plot of homozygosity in affected individuals compared with controls. Homozygosity scores are calculated by Homozygosity Mapper (7) from SNP genotype data and indicate a maximum score of 84 at a single location in the genome at chromosome 4q21.21. The *y* axis indicates homozygosity score, whereas the *x* axis shows location within the genome, organized by the chromosome. (*B*) Distribution of genotypes within FT1 for the region with the strongest evidence of homozygosity. (*Upper*) Homozygosity scores and location of *FGF5*, with the *x* axis indicating SNP marker positions on chromosome 4. (*Lower*) Split into affected and unaffected family members with each genotyped marker as a separate point on the *x* axis and individuals on the *y* axis. Genotype marker positions align with chromosomal location in the "affected" half. Genotypes are color coded, with heterozygous regions shown in blue, and homozygous regions in red. Notably, the region under *FGF5* is completely homozygous (red) in affected individuals, but heterozygous (red and blue) in unaffected individuals. (*C*) Whole exome sequencing results from FT1 and FT2. Our filtering strategy identified a single gene, *FGF5*, which contained, to our knowledge, novel damaging variants in both families. (*D*) Gene structure of *FGF5* shows that there are two alternatively spliced isoforms, *FGF5* (*Upper*) and *FGF5S* (*Lower*). In *FGF5S*, exon 2 (E2) is skipped, and a frameshift due to the out-of-frame splicing means the termination codon (TAG) is located only 14 base pairs into exon 3 (E3). Whereas c.159_160delTA, detected in FT2, is located in exon 1 (E1), and therefore affects both *FGF5* and *FGF5S*, the other two mutations only affect *FGF5*, as indicated by the positioning of the asterisks on the gene.

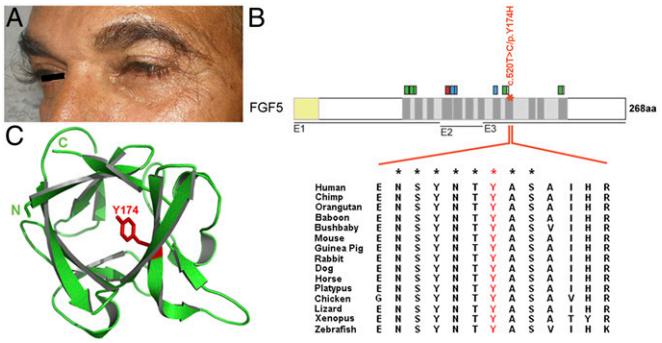

Fig. 3. Consequences of *FGF5* missense mutation on protein structure. (*A*) Clinical presentation of proband in FT3. (*B*) The rectangular boxed structure represents the protein structure of FGF5, which is 268 amino acids long. The mutation in FT3, which only affects *FGF5*, not *FGF5S*, is indicated with an orange asterisk. At the N terminus of FGF5 there is a signal peptide (yellow). FGF5 is composed of a highly conserved core region (gray) containing 12 β strands (dark gray), the coding sequence for which spans all three exons (E1–E3), and a signal peptide (yellow) at the N terminus. The core region has binding domains that interact with FGFR and are graphically illustrated above the protein diagram in green (interact with D2 on FGFR), red (interact with alternately spliced D3 on FGFR), blue (interact with D3 on FGFR), or gray (linker regions). The missense mutation identified in FT3 converts the tyrosine residue Y174, which is conserved in FGF5 across vertebrate species, to histidine. Conserved amino acids are indicated by asterisks at the top of the columns. (*C*) The structure of the core domain from FGF20, a close FGF5 homolog, is shown as a ribbon diagram. The side chain of Y174, mutated in FT3, is positioned within the hydrophobic core (and shown in red), with little surface exposure. Tyrosine is a hydrophobic side chain, whereas histidine is highly hydrophilic. We predict that p.Y174H will impact FGF5 function, so it has a reduced ability to bind and activate its receptor, FGFR1.

either fail to bind to and activate its receptor, FGFR1, or do so at significantly reduced levels.

Localization of FGF5 in the Hair Follicle. FGF5 acts as a stimulus for catagen entry by binding to FGFR1 located within the dermal papilla, a mesenchymal signaling center located at the base of the hair follicle (17). However, the origin of FGF5 has not been clearly established within mouse skin. One hypothesis is that FGF5 originating within the hair follicle outer root sheath acts to induce catagen (18), or alternatively, the source may reside in the follicle macroenvironment, potentially from FGF5-expressing macrophages that surround the hair follicle (19). To localize the isoforms of FGF5 in normal human hair follicles, we used PCR to amplify fragments of FGF5, and FGF5S in tissue from an unaffected individual, and found that both were expressed within occipital scalp skin in addition to plucked hair fibers (Fig. S4*A*). Immunohistochemistry on scalp skin also confirmed the presence of FGF5 within the upper outer root sheath cells of human hair follicles, and interestingly, in small round cells surrounding the follicle (Fig. S4*B*). In mouse skin, global changes in the macroenvironment have been shown to modulate hair cycling, which occurs in a synchronized wave (20). In contrast, human hair growth occurs in a mosaic pattern, not in a synchronized wave, and fluctuations in the macroenvironment have yet to been characterized. The presence of FGF5 in adjacent perifollicular cells invites further exploration of the role of these cells in the human hair cycle.

We took advantage of the localization of FGF5 within the outer root sheath to interrogate whether FGF5 protein was present within FT hairs. When a hair fiber is plucked from the skin it contains one to two layers of outer root sheath cells that remain attached to the hair. We performed whole mount immunofluorescence using patient and unaffected control plucked forearm hair fibers, with antibodies specific for both FGF5 and FGF5S. In FT1, we found that FGF5 was completely absent, and very low levels of detectable FGF5S were present, whereas in FT2 neither FGF5 nor FGF5S were present in the tissue surrounding plucked hair fibers, consistent with the predicted mechanism of action of the mutations (Fig. S5).

Phenotypical Effect of Mutations in FGF5. To our knowledge, this study is the first description of FGF5 gene mutations that are causative for trichomegaly in humans. Previously, mutations in FGF5 were found to be causative for the *angora* mouse phenotype (21), which is characterized by an abnormally long body hair coat (22). Within our families, hair growth was most striking on the eyelashes. However, to determine the impact of *FGF5* mutations on body hairs (Fig. S6), we obtained and measured plucked forearm hair fibers from adult male members of families FT1 and FT2. Not only were hairs significantly longer than those collected from controls, but they also showed an increased variance in length, which suggests that there is a dysregulation of a physiological process (Fig. 4*A*). However, hairs from affected family members were not any thicker than control hair fibers. We later categorized plucked hair fiber root tips into either anagen or telogen based on their morphology and found a notable shift in the anagen:telogen ratio toward anagen, in patient hairs compared with ethnically matched controls (Fig. 4*B*). In FT1, 65% of fibers were in anagen, and in FT2, 59% were in this cycle stage. This was compared with only 17% of control hair fibers being in anagen (83% in telogen), indicating that in humans, mutations in *FGF5* do not only affect eyelash hair follicles but also affect hair growth at other sites that predominantly reside in telogen, such as the forearm. Whereas mutations in *FGF5* result in longer hair fiber length, we cannot exclude the possibility that affected hair fibers are also growing faster than shorter hairs from control individuals. Longer eyelashes have previously been shown to have both a longer anagen duration, and a faster rate of growth than short eyelashes, with both of these features contributing to the observed length (23).

Overexpression of FGF5 in Human Hair Follicles Induces Catagen. In mouse skin, exogenous introduction of FGF5 by s.c. injection of recombinant proteins has previously been shown to induce premature entry into catagen, whereas FGF5S introduction can antagonize this effect (24), presumably by competitively binding the FGF5 receptor, FGFR1 (11). To assess the effect of FGF5 on the human hair cycle, we used the well-established organ culture model (25) for hair fiber elongation and grew microdissected human scalp hair follicles in the presence of recombinant FGF5 (Fig. 4*C*). Strikingly, the human follicles entered catagen prematurely after 2–4 d in the presence of recombinant FGF5, whereas untreated hairs entered catagen after 5–7 d (Fig. 4*D*). Their growth was significantly ($P = 0.03$) reduced after incubation with recombinant FGF5 protein, allowing us to conclude that, whereas a lack of FGF5 results in increased hair length as seen in our patients, overexposure to FGF5 inhibits hair growth in an organ culture model by initiating catagen.

Discussion

The *Angora* phenotype in mice is characterized by an abnormally long hair coat due to a prolonged anagen phase (lack of catagen onset) and a disrupted anagen:telogen ratio (22), with the phenotype resulting from a series of allelic mutations in *FGF5* (21). Subsequent to identification of *FGF5* as causative for the *angora* mouse phenotype, genetic variants in *FGF5* have been shown to underlie hair length regulation in several other species including cats, dogs, and even rabbits (26–28). However, until now, the human counterpart to the *angora* phenotype had remained elusive, and had not been described. Moreover, as the *angora* phenotype presents predominantly as extreme eyelash growth in

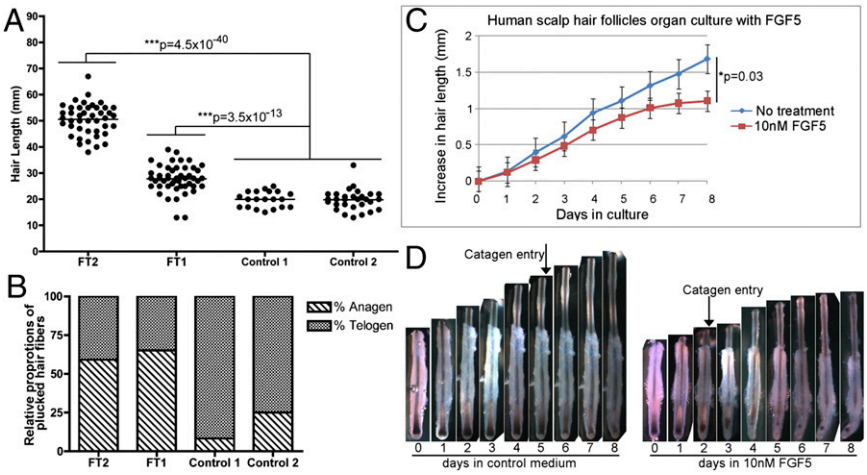

Fig. 4. Perturbations in FGF5 modulates hair fiber length and the anagen:telogen ratio of follicles. (*A*) Hair was plucked from the forearm of one affected adult male in FT1 and one affected male in FT2, then compared with hair from two separate ethnically matched controls. Each black dot represents an individual hair fiber, whereas the horizontal line is an average of all hair lengths per individual. An *F* test to measure variance within the sample indicated a greater variance (FT1 versus control $P = 7 \times 10^{-3}$, FT2 versus control $P = 7 \times 10^{-4}$) in the length of affected samples compared with controls, whereas an unpaired *t* test (*P* values indicated across top of graph) to assess the distribution of hair lengths indicated that the patient hair samples were significantly longer than control hair fibers. (*B*) The root tip morphology of plucked fibers were assessed and fibers were categorized into either anagen or telogen. There was a shift in the anagen:telogen ratio with an increased percentage of anagen hairs plucked from patient forearms, compared with ethnically matched controls. (*C*) Organ cultures of scalp hair follicles in control medium or medium containing 10 nM FGF5 were assessed and measured each day for 8 d. The lines on the graph depict the average (mean) increase in length of hair fibers in either control medium or FGF5, whereas the error bars are based on SE from the mean. We observed a significant decrease in follicle growth rate for hairs grown in medium containing FGF5 compared with controls. (*D*) Macroscopic images of hair follicles, either in control medium or FGF5 medium on days 0 through 8. In cultures containing FGF5, catagen entry, as determined by the shape of the end bulb (43), was earlier than in control cultures, explaining the observed reduction in growth rate.

humans, this study, to our knowledge, is the first identification of genetic mutations that underlie trichomegaly.

On the eyelashes, only ~15–40% of follicles are in anagen (29), while on body sites such as the upper arm or thigh, the percentages are even lower, giving these sites a relatively low anagen:telogen ratio (2). This is in contrast to body sites with very long hair, such as the scalp, where 85–95% of follicles are in anagen at any given time (30). The *angora* phenotype in mice is typically characterized by an extended anagen/delayed catagen, and an increased anagen:telogen ratio. Therefore, the most visible effects of mutations in *FGF5* will be observed on body sites that usually have short hair, with a high proportion of follicles in telogen, because these follicles now remain in anagen and continue fiber production. In our FT family members, the phenotype is most striking on the eyelashes.

In mouse skin, exogenous introduction of FGF5 by s.c. injection of recombinant proteins can induce premature entry of anagen hair follicles into catagen (24). Likewise, here we have demonstrated using human organ culture that exogenous FGF5 induces catagen in human hair as well. In the affected FT family members, we postulate that mutations in *FGF5* lead to loss of the stimulus for catagen entry, which in turn results in the prolonged anagen phenotype, and elongated eyelashes. Interestingly, many investigators have sought to identify anagen-stimulating agents that would promote longer hair growth. Here, we have found instead that loss of a catagen initiator results indirectly in longer hair growth by extending anagen, perhaps inviting future therapeutic targeting of catagen initiators to extend the anagen phase.

Bimatoprost is currently the only US Food and Drug Administration approved therapeutic intervention to increase the growth of eyelashes. Its effect on eyelash growth was discovered as a serendipitous side effect in patients being treated with it for ocular hypertension (31). Similarly, the effect of minoxidil (Rogaine) on hair growth was also discovered as a side effect of patients taking this drug for hypertension (32, 33). Common variants upstream of *FGF5* have been implicated in three genome-wide association studies of blood pressure ($3 \times 10^{-14} \leq P \leq 9 \times 10^{-25}$) (34–36) and replicated in independent cohorts (37, 38). A mechanistic link between *FGF5* variants associated with blood pressure and hair growth awaits further investigation.

In this study, we used a combined approach of homozygosity mapping together with whole exome sequencing to identify, to our knowledge, the first human counterpart of the *angora* phenotype. Further, we show that FGF5 is a key determinant of the anagen:telogen ratio, and hair length, in human hair follicles. These findings suggest that targeting FGF5 may be useful for two therapeutic approaches. First, because FGF5 initiates catagen in a growing hair follicle, an FGF5 agonist could be used for removal of unwanted or excess hair. Second, because inhibition of FGF5 can promote hair growth in eyelash hairs, we postulate that if the same mechanisms are operative in scalp hair follicles, perhaps inhibition of FGF5 could provide therapeutic benefit for patients with short anagen syndrome (39). Moreover, because this phenotype is strikingly visible in the eyelashes, it raises the possibility of therapeutic targeting of FGF5 to selectively enhance eyelash growth.

Materials and Methods

Patient Blood Collection. Informed consent, for blood/hair collection and taking and using photographs, was obtained from all subjects and approval for this study was provided by the Institutional Review Board of Columbia University. Peripheral blood samples were collected from family members, as well as unrelated healthy control individuals of Pakistani origin (50 individuals). Genomic DNA was isolated from these samples using the Puregene DNA isolation kit (Gentra System). We collected DNA from 21 members of FT1 and 9 members of FT2. We also collected DNA from probands of five other families who presented with trichomegaly.

Genome-Wide Linkage and Homozygosity Analysis. At the beginning of our study, we only had DNA from 14 of the 21 members of FT1. To identify regions in the genome with evidence for linkage and/or homozygosity, genome-wide SNP-based genotyping was performed on these original 14 members using the Affymetrix Human Mapping 10K 2.0 Array according to the

GENETICS

manufacturer's protocol. Quality control and data analysis was initially performed with Genespring GT (Agilent software). SNPs with greater than 5% missing data or SNPs that violated a Mendelian inheritance pattern were removed from the dataset before analysis. To reduce type I error introduced by linkage disequilibrium between markers, haplotypes were inferred from genotype data and analyzed for linkage under the assumption of a fully penetrant disease gene with a frequency of 0.001 transmitted by a dominant mode of inheritance. Homozygosity Mapper was used to identify homozygous regions shared among affected individuals (7). In Homozygosity Mapper, the homozygosity score is calculated as a function of marker genotype, sample size, and length of homozygous block. The score is relative and analysis dependent. In a single analysis, a homozygosity score is computed for each marker. A "maximum score" is also yielded in this process, which marks the region(s) of the genome with the highest level of homozygosity in a particular analysis (7).

Whole Exome Capture Followed by Massive Parallel Sequencing. Two members of FT1, three members of FT2, and five ethnically matched controls were subject to whole exome sequencing. Agilent SureSelectXT Human All Exon v.2 44 Mb kit (Agilent) was used for exome capture, which were then analyzed by massively parallel sequencing on an Illumina HiSEq 2000. Briefly, for each sample, fragment libraries were constructed using 3 μg of genomic DNA as starting material, following the Agilent standard library preparation protocol for Illumina TruSeq. A total of 500 ng of captured library was hybridized with the baits for 48 h, then washed and eluted using the Agilent protocol. Real-time PCR was used to quantify the libraries, which were subsequently sequenced with standard protocols for the Illumina HiSEq 2000 instrument. Standard Illumina TruSeq multiplexing (barcoding) protocol was used to sequence multiple samples in one lane.

Bioinformatics Analysis. Paired-end reads (read size: 101 bp) were mapped to the human reference genome National Center for Biotechnology Information (NCBI) build 37 using BWA (40) (version 0.5.9), allowing up to five mismatched, inserted or deleted bases (indels). Alignment was then refined using GATK (41) (version 1.0.6020) by performing local multiple sequence alignment around inferred putative indels and known ones from the 1000 Genomes Project, and subsequently recalibrating base quality scores. We then called single nucleotide variants (SNVs) and indels jointly from all of the samples in one batch of experiments using GATK (Unified Genotyper). In addition to the default variant filters in GATK, we applied additional filters to ensure low false discovery rate. These filters included: (*i*) number of reads that have zero-mapping quality is more than 10% of all of the reads mapped to the locus, or (*ii*) genotype quality score smaller than 30, or (*iii*) quality over depth less than 5.0, or (*iv*) strand bias score larger than −0.1. In total, this method allows us to detect about 17,000–20,000 coding SNVs, with an average transition to transversion ratio of 3.3 for known coding variants and 2.9 for novel coding variants, which indicates low false discovery rate (41). Called variants were annotated with Annovar and filtered under a recessive model for potentially damaging coding and splice site variants (3).

Sequence Validation. Exome sequencing validation was performed for FT1 and FT2 in individual exons. All three exons were also sequenced in affected probands from an additional five index cases with familial trichomegaly. Individual exons were amplified using Platinum PCR SuperMix (Invitrogen) and the following primers: exon 1 forward (5′-CTACAGAGCCCAGAATCAGC-3′) and reverse (5′-CCTACAAAACCCGTC CTAGG-3′), exon 2 forward (5′-CACAATGATATAAATAAGAGCCTG-3′) and reverse (5′-AAATTATTACTTCTG-GAAGCGCAC-3′), and exon 3 forward (5′-GATCGCCACAACTTAAATTTCC-3′) and reverse (5′-TTTCTCACAAGGCCAAGAGG-3′). Amplified PCR products were purified, then sequenced using the forward primer in an ABI Prism 310 Automated Sequencer, using the ABI Prism Big Dye Terminator Cycle Sequencing Ready Reaction kit (Invitrogen).

Statistical Analyses of Causal Variants. Two-point linkage analysis was performed for the disease variants with Superlink Online v1.5 (42). Data from all family members whose DNA was available for genotyping were included in the analysis. A fully penetrant disease allele with a population frequency of 0.001 and a recessive mode of inheritance was assumed based on studies in animal models. Variant burden for FGF5 in our cohort of FT families was calculated with Fisher's exact test, comparing the distribution of rare FGF5 variants in seven index cases (two index cases from FT1 and FT2 and five additional index cases) to those reported in the National Heart Lung and Blood Exome Sequencing Project (8).

Functional Predictions of Nonsynonymous Mutations. The crystal structure of FGF5 was based on a close protein homolog, FGF20. PyMol was used to generate a ribbon diagram of the protein, with the location of the substituted amino acid highlighted. We used three functional mutation prediction programs to determine the effect of p.Y174H on the protein. Polyphen-2 (14) generates a qualitative prediction based on sequence, phylogenetic, and structural information, with output scores close to 1 confidently predicting a damaging mutation. The program SIFT (16) predicts if mutations are deleterious or tolerable based on both sequence homology and the physical properties of amino acids. A score close to 0 is predicted to be highly deleterious. Lastly, Mutation Assessor (15) creates a functional impact score based on amino acid conservation, with scores above 1.9 indicating mutations that are predicted to have a medium or high impact on the protein function.

Plucked Hair Fiber Analysis. Hair fibers were plucked from the forearm of one affected adult male in FT1, one affected adult male in FT2, and two ethnically matched adult male controls. Individual hairs were straightened to extend, and measured in millimeters from the root tip through to the tapered end under a dissecting microscope. Broken hairs were discarded, leaving a lower number of total hair fibers that were used (48 from FT1, 43 from FT2, and 20 and 29, respectively, from the controls) in the final analysis. We calculated variance between samples using an *F* test and then assessed if there were significant differences in hair length between patient and control hairs using an unpaired two-tailed *t* test.

Fibers were also categorized into either anagen, or telogen groups based on the morphology of the root tip end. Anagen fibers have an elongated end, and often appear curled, or distorted at their tip. Comparatively, telogen fibers have a club shaped root tip. Percentages of fibers in either anagen or telogen were then calculated for affected males and controls.

Hair Follicle Organ Culture. Hair follicles were obtained as discarded tissue after hair transplantation procedures, in accordance with Helsinki guidelines after approval from the Columbia University Institutional Review Board. Follicles were microdissected from intact scalp skin, carefully cleaned of excess tissue, and transected just below the site of attachment of the sebaceous gland to the follicle. Each follicle was cultured in 1 well of a 24-well plate containing Williams Medium E (Sigma-Aldrich) supplemented with 2 mM glutamine, 1× antibiotics-antimycotics, 10 ng/mL hydrocortisone, and 10 mg/mL insulin. Recombinant long form FGF5 (R&D Systems) was reconstituted in sterile PBS containing 1 μg/mL heparin and 0.1% BSA for a stock solution of 10 μg/mL. For treatment of hair follicles, recombinant FGF5 was used, diluted 1/1,000, for a working concentration of 10 μg/μL. Control follicles were cultured in medium with the addition of heparin and BSA only. Follicles from two different control individuals were used in this analysis, for a total of 8 control follicles, and 10 follicles treated with FGF5. Media was changed every 3 d, but follicles were photographed each day to measure fiber growth rates. Fiber lengths were measured in millimeters, as the total height of the follicle with the new fiber, minus the starting height, and plotted as a growth rate graph using Microsoft Excel. Error bars were based on SE, whereas an unpaired two-tailed *t* test was performed on follicles at day 8, to compare differences between follicles in the treatment (FGF5) group versus control hair follicles.

PCR. Primers were designed against the FGF5 sequence deposited in the NCBI database (NM_004464). A forward primer (5′-CGCTATGTCTTCCTCTTCTGC-3′) was designed within the first exon of FGF5 and a reverse primer, spanning exons 1 and 2 (5′-CAAAACACTTAACATATTGGCTTCG-3′) to amplify FGF5, or spanning exons 1 and 3 (5′-TGAACTTGGCTTAACATATTGGC-3′) to amplify FGF5S. Forward (5′-CTCGGAGGATGATGATGATG-3′) and reverse (5′-CCTCC AATTCTGTGGTCAGG-3′) primers for the FGF5 receptor, FGFR1, were also designed. Finally, forward (5′-CACAGCCCAAGATAGTTAAGTG-3′) and reverse (5′-GCATAAAGTGTAAGTGTATAAGCATA-3′) beta-2-microglobulin primers were used as housekeeping controls. PCR was performed on cDNA from whole scalp skin, plucked hair fibers, microdissected dermal papillae, whole blood peripheral blood mononuclear cells, and T cells isolated from blood. cDNA was amplified using Platinum PCR Supermix for 30 cycles, with an annealing temperature of 55 °C, and a 30-s extension at 72 °C. Products were separated on 2% (wt/vol) agarose gels.

Whole Mount Immunofluorescence. To perform whole mount immunofluorescence, plucked forearm hair fibers from affected males in FT1 and FT2, or from ethnically matched controls, were adhered to microscope slides using crazy glue, leaving the root tips exposed on the lower half of the slide. Hairs were rehydrated for 15 min in PBS pH 7.4 before fixation for 10 min in 4%

paraformaldehyde. Hairs were then washed in 3 × 10 min washes of PBS and placed in blocking solution [2% (wt/vol) fish skin gelatin, 1% (vol/vol) donkey serum, 0.5% Triton X-100 in PBS] for 1 h. Primary antibodies were applied overnight at 4 °C in a humidified chamber, both diluted 1/100. We used two FGF5 antibodies; a polyclonal antibody D01P (Abnova), raised against amino acids 1–123, predicted to recognize both FGF5 and FGF5S, and a polyclonal antibody (Abbiotec) that recognizes a 27-amino-acid epitope at the C terminus, and therefore recognizes only FGF5, not FGF5S. After primary antibody incubation, hairs were washed 3 × 10 min in PBS, and a donkey anti-rabbit 488-conjugated secondary antibody (Molecular Probes) at 1:800 was applied for 1 h at room temperature. Antibodies were washed off for 3 × 10 min in PBS, and coverslips applied using Vectashield containing DAPI (Vector Labs). Hairs were visualized on a LCM Excitor confocal microscope (Zeiss) and both patient and control hairs were photographed under the same conditions.

Immunohistochemistry. For immunohistochemistry to localize FGF5, we used 8-μM paraffin sections of normal occipital scalp tissue adhered to positively charged slides. Slides were deparaffinized with xylene then rehydrated through decreasing gradients of ethanol. Antigen retrieval was performed by placing slides in boiling sodium citrate buffer (pH 6) for 5 min, then allowed to cool to room temperature. Slides were washed in Tris-buffered saline pH 8.4 (3 × 3 min), then incubated with blocking solution [2% (vol/vol) goat serum, 1% (wt/vol) BSA, 0.1% fish skin gelatin, 0.1% Triton X-100, and 0.05% Tween-20 in TBS] for 1 h. A primary antibody against FGF5 (Abbiotec) was diluted 1/100 and incubated on slides overnight at 4 °C in a humidified chamber. After washing off primary antibody with 3 × 3 min PBS washes, a secondary antibody, biotin-XX goat anti-rabbit (Molecular Probes) at 1/1000 was applied for 45 min. This was washed off with TBS, and a tertiary, streptavidin-alkaline phosphatase (Zymed) at 1/300 was applied for 30 min at room temperature. Slides were washed and alkaline phosphatase was visualized using Sigma Fast Red (Sigma) for ∼10 min. Slides were washed and counterstained using Hematoxylin QS (Vector Labs) before mounting coverslips using glycergel.

ACKNOWLEDGMENTS. We are grateful to the family members for their participation in this study; Ms. Helen Lam for technical assistance; Dr. Ali Jabbari for insightful discussions; and the Columbia Sulzberger Genome Center and the Center for Computational Biology and Bioinformatics at Columbia University. This study was supported by a US Public Health Service/National Institutes of Health Grant (RO1AR44924) from the National Institute of Arthritis and Musculoskeletal and Skin Diseases (to A.M.C.). C.A.H. and S.H. were supported by Dermatology Foundation Science of Human Appearance Career Development awards.

1. Alonso L, Fuchs E (2006) The hair cycle. *J Cell Sci* 119(Pt 3):391–393.
2. Seago SV, Ebling FJ (1985) The hair cycle on the human thigh and upper arm. *Br J Dermatol* 113(1):9–16.
3. Wang K, Li M, Hakonarson H (2010) ANNOVAR: Functional annotation of genetic variants from high-throughput sequencing data. *Nucleic Acids Res* 38(16):e164.
4. Gray H (1944) Trichomegaly or movie lashes. *Stanford Med Bull* 2:157–158.
5. Paul LJ, Cohen PR, Kurzrock R (2012) Eyelash trichomegaly: Review of congenital, acquired, and drug-associated etiologies for elongation of the eyelashes. *Int J Dermatol* 51(6):631–646; quiz 643-634, 646.
6. Harrison DA, Mullaney PB (1997) Familial trichomegaly. *Arch Ophthalmol* 115(12):1602–1603.
7. Seelow D, Schuelke M, Hildebrandt F, Nurnberg P (2009) HomozygosityMapper: An interactive approach to homozygosity mapping. *Nucleic Acids Res* 37(Web Server issue):W593–W599.
8. Boyden LM, et al. (2012) Mutations in kelch-like 3 and cullin 3 cause hypertension and electrolyte abnormalities. *Nature* 482(7383):98–102.
9. Plotnikov AN, Hubbard SR, Schlessinger J, Mohammadi M (2000) Crystal structures of two FGF-FGFR complexes reveal the determinants of ligand-receptor specificity. *Cell* 101(4):413–424.
10. Clements DA, Wang JK, Dionne CA, Goldfarb M (1993) Activation of fibroblast growth factor (FGF) receptors by recombinant human FGF-5. *Oncogene* 8(5):1311–1316.
11. Ozawa K, et al. (1998) An alternatively spliced fibroblast growth factor (FGF)-5 mRNA is abundant in brain and translates into a partial agonist/antagonist for FGF-5 neurotrophic activity. *J Biol Chem* 273(44):29262–29271.
12. Plotnikov AN, Schlessinger J, Hubbard SR, Mohammadi M (1999) Structural basis for FGF receptor dimerization and activation. *Cell* 98(5):641–650.
13. Pellegrini L, Burke DF, von Delft F, Mulloy B, Blundell TL (2000) Crystal structure of fibroblast growth factor receptor ectodomain bound to ligand and heparin. *Nature* 407(6807):1029–1034.
14. Adzhubei I, Jordan DM, Sunyaev SR (2013) Predicting functional effect of human missense mutations using PolyPhen-2. *Curr Protoc Hum Genet* Chapter 7:Unit7.20.
15. Reva B, Antipin Y, Sander C (2011) Predicting the functional impact of protein mutations: Application to cancer genomics. *Nucleic Acids Res* 39(17):e118.
16. Kumar P, Henikoff S, Ng PC (2009) Predicting the effects of coding non-synonymous variants on protein function using the SIFT algorithm. *Nat Protoc* 4(7):1073–1081.
17. Ota Y, et al. (2002) Fibroblast growth factor 5 inhibits hair growth by blocking dermal papilla cell activation. *Biochem Biophys Res Commun* 290(1):169–176.
18. Pena JC, Kelekar A, Fuchs EV, Thompson CB (1999) Manipulation of outer root sheath cell survival perturbs the hair-growth cycle. *EMBO J* 18(13):3596–3603.
19. Suzuki S, et al. (1998) Localization of rat FGF-5 protein in skin macrophage-like cells and FGF-5S protein in hair follicle: Possible involvement of two Fgf-5 gene products in hair growth cycle regulation. *J Invest Dermatol* 111(6):963–972.
20. Jahoda CA, Christiano AM (2011) Niche crosstalk: Intercellular signals at the hair follicle. *Cell* 146(5):678–681.
21. Hébert JM, Rosenquist T, Götz J, Martin GR (1994) FGF5 as a regulator of the hair growth cycle: Evidence from targeted and spontaneous mutations. *Cell* 78(6):1017–1025.
22. Pennycuik PR, Raphael KA (1984) The angora locus (go) in the mouse: Hair morphology, duration of growth cycle and site of action. *Genet Res* 44(3):283–291.
23. Thibaut S, et al. (2010) Human eyelash characterization. *Br J Dermatol* 162(2):304–310.
24. Suzuki S, Ota Y, Ozawa K, Imamura T (2000) Dual-mode regulation of hair growth cycle by two Fgf-5 gene products. *J Invest Dermatol* 114(3):456–463.
25. Philpott MP, Green MR, Kealey T (1990) Human hair growth in vitro. *J Cell Sci* 97(Pt 3):463–471.
26. Drögemüller C, Rüfenacht S, Wichert B, Leeb T (2007) Mutations within the FGF5 gene are associated with hair length in cats. *Anim Genet* 38(3):218–221.
27. Cadieu E, et al. (2009) Coat variation in the domestic dog is governed by variants in three genes. *Science* 326(5949):150–153.
28. Kehler JS, et al. (2007) Four independent mutations in the feline fibroblast growth factor 5 gene determine the long-haired phenotype in domestic cats. *J Hered* 98(6):555–566.
29. Elder MJ (1997) Anatomy and physiology of eyelash follicles: Relevance to lash ablation procedures. *Ophthal Plast Reconstr Surg* 13(1):21–25.
30. Rook A (1965) Endocrine influences on hair growth. *BMJ* 1(5435):609–614.
31. Cohen JL (2010) Commentary: From serendipity to pilot study and then pivotal trial: Bimatoprost topical for eyelash growth. *Dermatol Surg* 36(5):650–651.
32. Pettinger WA (1980) Minoxidil and the treatment of severe hypertension. *N Engl J Med* 303(16):922–926.
33. Mehta PK, Mamdani B, Shansky RM, Mahurkar SD, Dunea G (1975) Severe hypertension. Treatment with minoxidil. *JAMA* 233(3):249–252.
34. Newton-Cheh C, et al.; Wellcome Trust Case Control Consortium (2009) Genome-wide association study identifies eight loci associated with blood pressure. *Nat Genet* 41(6):666–676.
35. Ehret GB, et al.; International Consortium for Blood Pressure Genome-Wide Association Studies; CARDIoGRAM Consortium; CKDGen Consortium; KidneyGen Consortium; EchoGen Consortium; CHARGE-HF Consortium (2011) Genetic variants in novel pathways influence blood pressure and cardiovascular disease risk. *Nature* 478(7367):103–109.
36. Wain LV, et al.; LifeLines Cohort Study; EchoGen Consortium; AortaGen Consortium; CHARGE Consortium Heart Failure Working Group; KidneyGen Consortium; CKDGen Consortium; Cardiogenics Consortium; CardioGram (2011) Genome-wide association study identifies six new loci influencing pulse pressure and mean arterial pressure. *Nat Genet* 43(10):1005–1011.
37. Xi B, et al. (2014) Association of common variants in/near six genes (ATP2B1, CSK, MTHFR, CYP17A1, STK39 and FGF5) with blood pressure/hypertension risk in Chinese children. *J Hum Hypertens* 28:32–36.
38. Xi B, Shen Y, Reilly KH, Wang X, Mi J (2013) Recapitulation of four hypertension susceptibility genes (CSK, CYP17A1, MTHFR, and FGF5) in East Asians. *Metabolism* 62(2):196–203.
39. Antaya RJ, Sideridou E, Olsen EA (2005) Short anagen syndrome. *J Am Acad Dermatol* 53(2, Suppl 1):S130–S134.
40. Li H, Durbin R (2009) Fast and accurate short read alignment with Burrows-Wheeler transform. *Bioinformatics* 25(14):1754–1760.
41. DePristo MA, et al. (2011) A framework for variation discovery and genotyping using next-generation DNA sequencing data. *Nat Genet* 43(5):491–498.
42. Silberstein M, et al. (2006) Online system for faster multipoint linkage analysis via parallel execution on thousands of personal computers. *Am J Hum Genet* 78(6):922–935.
43. Khidhir KG, et al. (2013) The prostamide-related glaucoma therapy, bimatoprost, offers a novel approach for treating scalp alopecias. *FASEB J* 27(2):557–567.